Instability and droplet formation in evaporating thin films of a binary solution

Leonid V. Govor,[1,*] Jürgen Parisi,[1] Gottfried H. Bauer,[1] and Günter Reiter[2]
[1]*Institute of Physics, University of Oldenburg, D-26111 Oldenburg, Germany*
[2]*Institut de Chimie des Surfaces et Interfaces, CNRS-UHA, 68057 Mulhouse Cedex, France*
(Received 5 January 2005; published 9 May 2005)

We consider an instability phenomenon in a bilayer structure resulting from phase separation in a thin film of mixed solutions located on a water surface. The top layer consists of a hexane/hexadecylamine solution with thickness d_2, the lower one of an amyl acetate/cellulose solution with thickness d_1. During evaporation of the solvents from both layers, their thickness, surface tension, and viscosity change continuously with time. The thickness d_2 decreases significantly faster than the thickness d_1, because the evaporation rate of hexane is much larger than that of amyl acetate. Eventually, the top layer decomposes into droplets when its thickness d_2 was only a few nm, while the thickness d_1 was still some 100 nm. In addition to the experiments, we present calculations based on energetic arguments which are in good agreement with experimentally determined geometrical parameters of the droplet pattern, such as droplet diameter, droplet height, interdroplet distance, and number of droplets per unit area.

DOI: 10.1103/PhysRevE.71.051603 PACS number(s): 68.08.Bc, 68.15.+e, 81.16.Rf, 68.55.−a

I. INTRODUCTION

For the fabrication of structures and devices with sizes below 30 nm, conventional electron-beam lithography becomes exceedingly difficult. Therefore, nanoparticles and mesoscopic arrangements formed with nanoparticles have gained increasing interest. The ordering of nanoparticles into micrometer-size structures that retain the unique nanoparticle properties can be used for the development of new functional materials and for the fabrication of a wide variety of nanodevices [1]. In this case, none of the traditional methods can be used to manufacture the ordered structure. Self-assembly of nanoparticles in a ringlike structure which occurred during the formation of a thin film of the polymer solution containing the particles was reported by various authors [2–6]. Recently, we have presented experimental evidence for the formation of self-assembled rings of $CoPt_3$ nanoparticles (ring diameter ranging from 0.6 to 1.5 μm, particle diameter 6 nm) developed in an evaporating thin film [7,8]. The latter was formed on a water surface by spreading a binary mixture composed of two solutions, namely nitrocellulose dissolved in amyl acetate and $CoPt_3$ particles stabilized by hexadecylamine dissolved in hexane. We found that phase separation in a thin spread film of the mixed solutions leads to a bilayer, and the subsequent solvent evaporation out of the top hexadecylamine solution layer favors its decomposition into droplets. Finally, evaporation of the remaining solvent from these droplets gives rise to a retraction of their contact line. The $CoPt_3$ particles located at the contact line follow its motion and self-assemble along this line.

In the present work, we analyze such an instability phenomenon in the thin bilayer structure of two different liquids on the water surface. The top layer consists of a hexane/hexadecylamine solution (HDA solution) with thickness d_2, the lower one of an amyl acetate/nitrocellulose solution (NC solution) with thickness d_1. During evaporation of the solvents out of both layers, their parameters such as thickness d_2 and d_1, surface tension, and viscosity change with time. The evaporation rate of hexane in the top HDA solution layer is significantly larger than that of amyl acetate in the NC solution layer. As a result, the thickness of the top layer just at the moment before it decomposes into droplets was only a few nm while the thickness of the bottom layer was still some 100 nm. In the following, we inspect the development of the instability in the ultrathin top HDA solution layer providing its rupture into micrometer-sized droplets in detail.

II. EXPERIMENT

We have used a blend (B) that contains 50% of a 1% nitrocellulose solution in amyl acetate and 50% of a solution of $CoPt_3$ particles (with a diameter of 6 nm) stabilized with HDA and dissolved in hexane [9]. The concentration of $CoPt_3$ particles in solution amounts to 17 mg/mL. Addition of HDA (7 mg/mL) to the suspension of the $CoPt_3$ particles in hexane leads to the formation of a clear stable colloidal solution of particles.

Spreading a 3 μL drop of the binary mixture of the solutions on the water surface in a Petri dish of 90 mm diameter (see in Fig. 1) was used for preparation of the thin film, which provided the basis for the droplet formation [10]. Total spreading of a drop of the blend solution B on the water surface is obtained due to the positive spreading coefficient [11] $S_{B/W}=\gamma_W-\gamma_B-\gamma_{B/W}=25.3$ mN/m. Here, $\gamma_W=72.5$ mN/m, $\gamma_B=22.8$ mN/m, and $\gamma_{B/W}=24.4$ mN/m give the surface tension at the interfaces between water and air (W), between blend and air (B), and between blend solution and water (B/W), respectively. The interfacial tension $\gamma_{B/W}$ was derived from the difference between the surface tension of water saturated with the polymer solution and that of the polymer solution saturated with water. The values of the surface tension were determined using a stalagmometer [12]. After evaporation of hexane and amyl acetate, the dry thin

*Email address: leonid.govor@uni-oldenburg.de

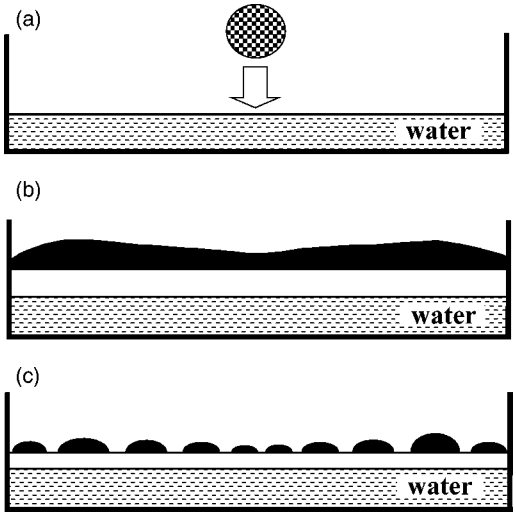

FIG. 1. Schematic illustration of the preparation procedure of a hexadecylamine droplet pattern. (a) Spreading of a drop of binary mixture on the water surface. (b) Formation of a bilayer structure: HDA solution layer (dark) above NC solution layer (bright). (c) Decomposition of the top HDA solution layer into droplets. The droplet diameter corresponds to the thickness of the HDA solution layer.

film was transferred onto a glass substrate. The topography of these solid thin films was analyzed by atomic force microscopy (AFM, model Burleigh Vista 100), and the arrangement of the $CoPt_3$ particles by transmission electron microscopy (TEM, model Zeiss EM 902).

III. EXPERIMENTAL RESULTS

We have found that a phase-separated structure of hexadecylamine islands containing $CoPt_3$ particles (hereafter called HDA droplets) was formed on a thin cellulose film. The size of the HDA droplets depends on the distance from the spreading center along the radius R of the spreading area. Within regions with a width of about 2–4 mm, located symmetrically around the spreading center, the size of the HDA droplets was approximately constant. For $R=0$, we observed the smallest HDA droplets with a height $h_d=5$ nm and diameter $D_d=0.65$ μm. For $R\approx 20$ mm, we found the largest HDA droplets with $h_d=23.5$ nm and $D_d=1.5$ μm. For all other values of R, h_d was in the range from 5 to 23.5 nm (corresponding to D_d in the range from 0.65 to 1.5 μm). In Figs. 2(a) and 2(b), we present AFM images (AC mode, topography) of a typical structure of the HDA droplets with the average droplet height $h_d=14.9$ nm and the corresponding average diameter $D_d=0.95$ μm. The average values of both droplet height and diameter have been estimated from the sizes of all droplets shown in Fig. 2(b). Figure 2(c) demonstrates that the height difference of the neighboring droplets can amount to up to 6 nm.

In order to end up with a better understanding of the formation mechanism of the droplet structure, we have determined the penetration depth of the droplets into the cellulose film. For this purpose, the HDA droplets were removed by immersing the sample for a period of 5 min in hexane, which

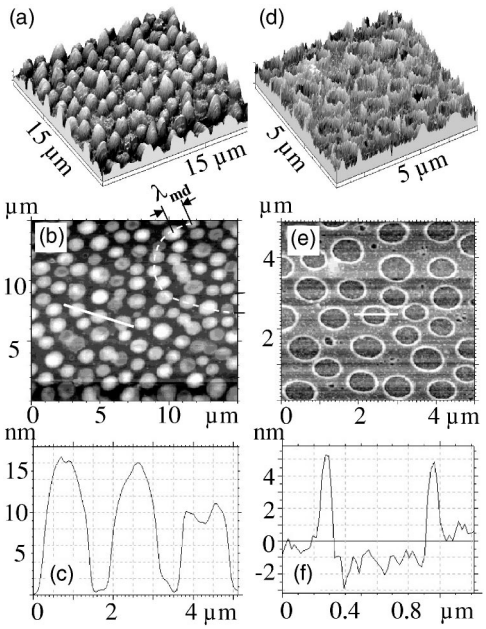

FIG. 2. (a) Three-dimensional and (b) two-dimensional AFM images of HDA droplets on a cellulose film with average diameter $D_d=0.95$ μm and average height $h_d=14.9$ nm. The additionally marked dashed curve in (b) indicates the arrangement of the droplets along this line. λ_{md} is the interdroplet distance within one line. (c) AFM profile of the scan line indicated in (b). (d) Three-dimensional and (e) two-dimensional AFM images of the cellulose layer after removal of the HDA droplets. (f) Profile of the scan line indicated in (e).

is a selective solvent for HDA. Figures 2(d) and 2(e) show typical AFM pictures of the remaining cellulose layer. We have found that the thickness of the underlying cellulose film was approximately constant, in the range of about 3–4 nm. Figure 2(f) clearly illustrates that the depth of depression, which remains in the cellulose film after removal of the HDA droplets, is only about 1 nm, and the height of a rim that surrounds the HDA droplet is about 5 nm. The latter indicates that the thickness of the cellulose film under depression amounts to at least 2–3 nm. Consequently, the HDA droplets have no contact with the substrate surface, i.e., the substrate is completely covered by the cellulose film.

Our TEM investigations of the droplet structure demonstrate that the $CoPt_3$ particles self-assemble into a ring pattern located at the perimeter of the HDA droplet. Figure 3(a) displays a TEM image of the droplet structure; Fig. 3(b) displays the single nanoparticle ring at the edge of a droplet with a diameter of 0.86 μm and an arrangement of the nanoparticles which we call one-dimensional (see inset). Within the spreading area, we can also observe regions where the droplets are still in contact with an unperturbed solid HDA film, which by far surmount the droplet size. Figure 3(c) exhibits a typical example of such a region where the $CoPt_3$ particles assemble at its edge. Figure 3(d) displays an area of an unfinished process of droplet formation.

Figure 2(b) indicates that the droplets tend to be arranged on curved lines (one of them is indicated by a dashed line). We have observed that the interdroplet distance within one line, λ_{md} [see Fig. 2(b)], and the droplet height h_d both de-

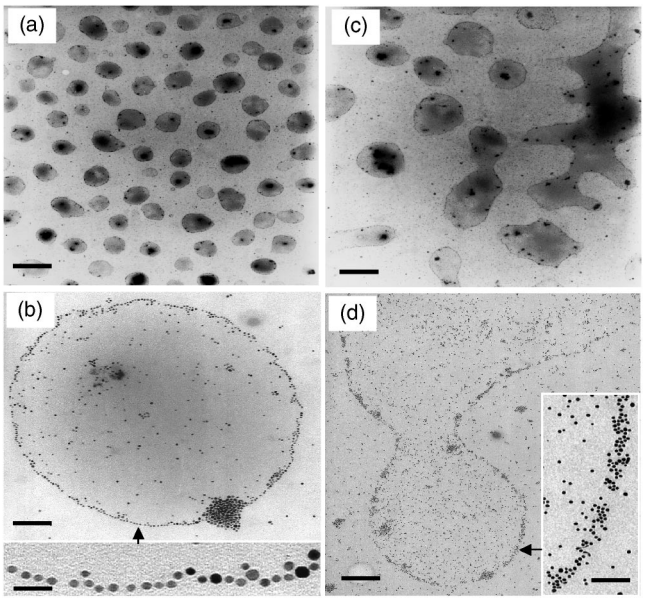

FIG. 3. TEM images of the HDA droplet structure with $CoPt_3$ particle rings formed at the edge of HDA droplets. (a) HDA droplets on the cellulose layer; scale bar 2110 nm. (b) Nanoparticle ring with one-dimensional assembling; scale bar 110 nm. The detailed structure is magnified in the inset; scale bar 25 nm. (c) Droplets located near the segment from which they were built; scale bar 1430 nm. (d) HDA segment with $CoPt_3$ particles assembling at its edge; scale bar 300 nm (70 nm in the inset).

pend on the droplet diameter D_d. In total, a series of 13 samples, with an average droplet diameter ranging from 0.65 to 1.5 μm, has been analyzed. For each sample, the values of the parameters λ_{md} and h_d of all droplets located inside an area of about 100 μm^2 were measured and the corresponding average values determined. The distributions of λ_{md} and h_d were centered around the corresponding average value with a standard deviation of 12% and 27%, respectively. The distribution width of each parameter turned out to be independent of the droplet diameter D_d. The average values of λ_{md} and h_d together with the corresponding standard deviations in the distribution (bars in figures) as a function of D_d are plotted in Fig. 4. We disclose the power-law dependences $\lambda_{md} \propto D_d^{m_1}$ and $h_d \propto D_d^{m_2}$ (the values of the exponents m_1 and m_2 are indicated in Fig. 4), i.e., the parameters λ_{md} and h_d change with the droplet diameter D_d. We like to emphasize that, in general, the power-law dependence of h_d on D_d is characterized by a stepwise increase of the droplet height with increasing diameter. Such steps can be clearly recognized in Fig. 4(b) for D_d values in the ranges from 0.7 to 1 μm and from 1.1 to 1.5 μm. A much stronger and abrupt change of h_d with increasing D_d becomes visible in the range from 0.65 to 0.7 μm.

In our experiments, we can observe only the droplet structure at the end of the evaporation process of a thin binary solution film. For the sake of understanding the droplet structure formation, it is interesting to know the relation between geometrical parameters of the droplet structure and the thickness h_f of the corresponding unperturbed HDA film in solid state, from which such droplet structure develops. In other

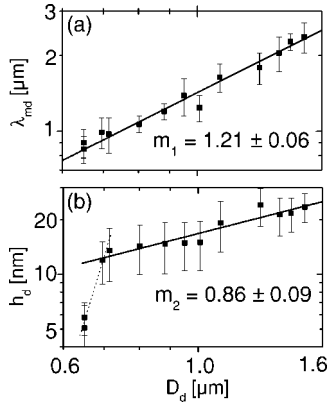

FIG. 4. Double logarithmic plots of the average values of (a) interdroplet distance λ_{md} within one line, and (b) droplet height h_d as a function of average droplet diameter D_d. The bars at each data point denote the corresponding standard deviation in the distribution.

words, it is necessary to find the dependences between the initial thickness h_f and parameters such as interdroplet distance λ_{md}, droplet height h_d, droplet diameter D_d, and droplet number N_d per area unit. For this purpose, we have calculated the HDA film thickness h_f from the total volume of all droplets N_d which are located on a 100 μm^2 area of each of the samples investigated. The resulting parameters as a function of h_f are plotted in Fig. 5. With the exception of the droplet height h_d, beginning from a "characteristic" film thickness $h_f \geqslant 2.4$ nm all parameters significantly depend on h_f, but for smaller values of h_f, these parameters are almost independent of h_f. In the following, we concentrate our discussion on the dependences in the range $h_f > 2.4$ nm. Figure 5(a) illustrates that the interdroplet distance λ_{md} undergoes a power-law dependence $\lambda_{md} \propto h_f^{n_1}$ with $n_1 = 2.03 \pm 0.21$. The

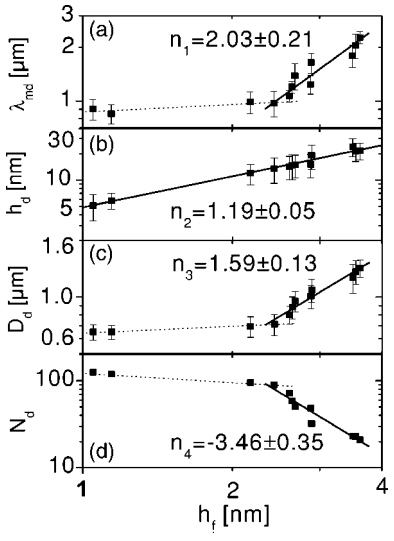

FIG. 5. Double logarithmic plots of the average values of (a) interdroplet distance λ_{md} within one line, (b) droplet height h_d, (c) droplet diameter D_d, and (d) number of droplets N_d located on a 100 μm^2 sample area as a function of HDA film thickness h_f. The bars at each data point denote the corresponding standard deviation in the distribution.

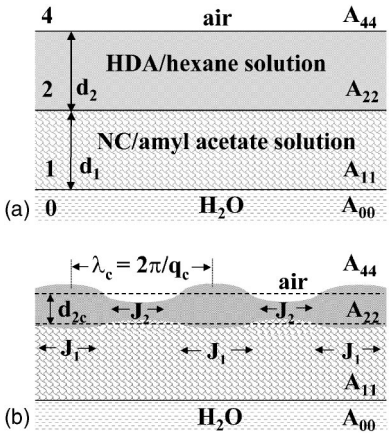

FIG. 6. Schematic illustration of the development of the phase-separated structure. (a) Formation of phase-separated layers (bilayer structure). The media 0, 1, 2, and 4 are water substrate, NC solution, HDA solution, and air, respectively. The designations A_{ii} refer to the corresponding Hamaker constants. d_2 and d_1 denote the thickness of the HDA solution and NC solution layers, respectively. (b) Development of the thickness fluctuations of the HDA solution layer. The designations are explained in the text.

measured power-law dependence $h_d \propto h_f^{n_2}$ with $n_2 = 1.19 \pm 0.05$ in the whole range of h_f investigated means that the droplet height increases about linearly with film thickness [Fig. 5(b)]. In contrast to that, the dependence D_d on h_f shows a change in behavior at the "characteristic" film thickness and, in the range $h_f > 2.4$ nm, the power-law dependence $D_d \propto h_f^{n_3}$ with $n_3 = 1.59 \pm 0.13$ comes out [Fig. 5(c)]. For the number of droplets per 100 μm^2 sample area, we unveil the strong dependence $N_d \propto h_f^{n_4}$ with $n_4 = -3.46 \pm 0.35$ [Fig. 5(d)].

IV. DISCUSSION

According to the experimental results shown in Fig. 2, we conclude that the initial thin layer of mixed solutions on the water surface transforms into a bilayer structure which consists of a hexane/hexadecylamine solution layer with thickness d_2 at the solution-air interface [layer 2 in Fig. 6(a)] and an amyl acetate/cellulose solution layer with thickness d_1 at the solution-water interface [layer 1 in Fig. 6(a)]. Assuming complete phase separation, the thickness of both liquid layers can be determined from the thickness h_f, the covered area, and the concentration of HDA and NC in the initial blend solution *B*. Before evaporation, the HDA solution layer contains 99.4% hexane and only 0.6% hexadecylamine; the corresponding NC solution layer contains 99% amyl acetate and only 1% cellulose. The number of $CoPt_3$ particles in each layer was about 6×10^{12}. For example, the sample with thickness $h_f = 2.7$ nm of the dry HDA layer could only be formed after evaporation of the liquid HDA solution layer with thickness $d_2 = 381$ nm. The thickness of the dry cellulose layer was about 3 nm in all samples investigated, resulting from a liquid NC solution layer with thickness $d_1 = 390$ nm. One reason for the formation of the bilayer is that the HDA solution with its lower surface free energy (18.4 mN/m for the HDA solution and 24.6 mN/m for the NC solution, respectively) wets the air surface, in order to minimize the free energy at the interface between air and solution [13–16]. The role of $CoPt_3$ particles in the formation of an HDA droplet structure was analyzed with a blend that contains 50% of a 1% NC solution in amyl acetate and 50% of a 1% HDA solution in hexane *without* the nanoparticles. We observed a rather similar HDA droplet pattern. That is, the $CoPt_3$ particles do not play a crucial role in the development of HDA droplets, and, in the following discussion, we will neither consider the attraction between nanoparticles in the solution nor that between nanoparticles and HDA solution.

The HDA solution wets the layer of the NC solution [see Fig. 6(a)] if the condition for the spreading coefficient $S_{21} = \gamma_1 - \gamma_2 - \gamma_{21} > 0$ is fulfilled. Here, γ_2 and γ_1 designate the surface tension of the HDA solution and that of the NC solution at the boundary between the corresponding phase and air, respectively; γ_{21} is the surface tension at the interface between the HDA solution and the NC solution. For a careful analysis of the evaporation process of the bilayer structure, we measured the values of the surface tension of both HDA and NC layers in the dry state. They were obtained from a so-called Zisman plot [17], where we determined the contact angle θ_c of the droplets (volume 1–3 μL) of water, glycerol, formamide, piridine, cyclohexanone, decalin, and *n*-decane on the surface of thin HDA and NC films deposited onto a glass substrate. We could not use alkanes as they would dissolve our layers. The choice of the fluids for capturing the critical surface tension was based on the following constraints: first, we had to cover a large interval of surface tension values for the Zisman plot, and second, the liquids must not dissolve HDA or NC solid layers. The resulting values of the surface tension of both HDA and NC layers in the dry state amount to $\gamma_{HDA} = 25.8 \pm 0.9$ mN/m and $\gamma_{NC} = 28.6 \pm 1.2$ mN/m, respectively.

The relation $\gamma_{HDA} < \gamma_{NC}$ is valid for both layers in the dry state. However, we do not know when in the course of evaporation the above relation becomes valid and whether this inequality is applicable for the entire duration of the evaporation process. Thus, in the following, we discuss the alteration of both parameters γ_2 and γ_1 during evaporation. First, we determined experimentally the evaporation rate of hexane (24 mL) by monitoring the mass losses versus time under geometrical and temperature conditions similar to those for the experiment using the binary solutions, and we found 3.30 ± 0.06 mg/s [see Fig. 7(a)]. The analogous evaporation rate estimated experimentally for amyl acetate (24 mL) was 0.16 ± 0.01 mg/s. Second, we derived the evaporation rate of the respective solvents from a mixture that contained 24 mL hexane and 24 mL amyl acetate. In the latter case, the evaporation process is divided into two distinct regimes: first, the evaporation of hexane at 2.45 ± 0.11 mg/s, and second, that of amyl acetate at 0.13 ± 0.01 mg/s. On the one hand, we found that the evaporation rate of hexane in the mixture is lower by 26% than that of pure hexane. The corresponding decrease of the evaporation rate of amyl acetate amounts to 19%. On the other hand, we observed that the evaporation rate of hexane (pure or in mixture) is about 20 times larger than that of amyl

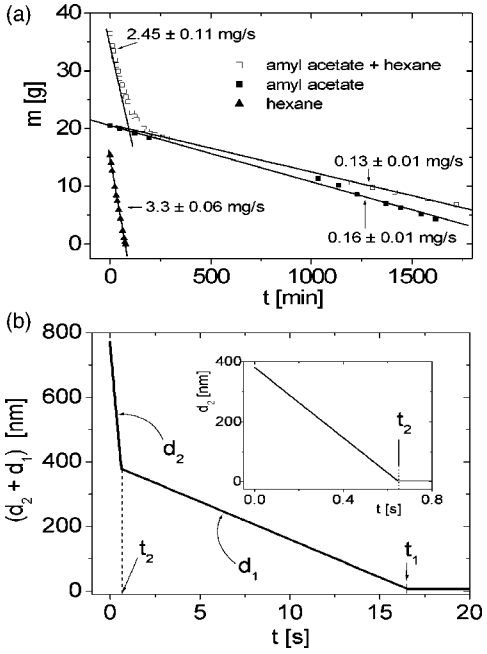

FIG. 7. (a) Time dependence of the evaporation of three solvents: two-phase solvent contained amyl acetate and hexane, pure amyl acetate, and pure hexane. The corresponding slope of the approximation lines (evaporation rate) is indicated in the figure. (b) Calculated thickness of both HDA solution (d_2) and NC solution (d_1) layers as a function of evaporation time for the sample with $h_f=2.7$ nm. The detailed analysis of the time dependence of thickness d_2 is magnified in the inset. The corresponding slope for the thickness d_2 amounts 589 nm/s and that for d_1 amounts 23.5 nm/s. $t_2=0.647$ s is the time period necessary for complete evaporation of hexane out of the top HDA solution layer, and $t_1=16.58$ s is the time period necessary for evaporation of amyl acetate out of the lower NC solution layer.

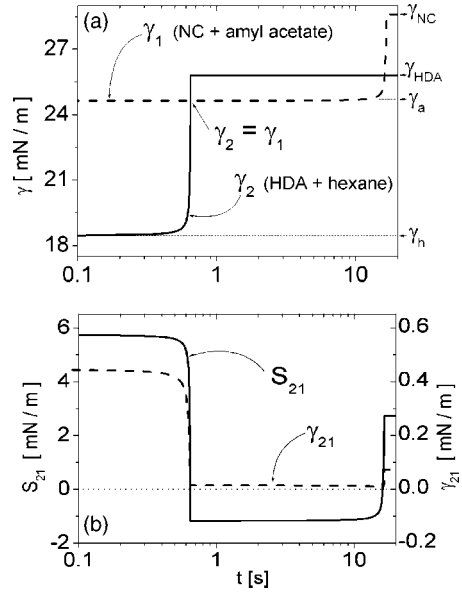

FIG. 8. (a) Calculated surface tensions versus evaporation time. The curve γ_2 characterizes the evaporation process of the HDA solution layer with $\gamma_h=18.4$ mN/m (hexane), $\gamma_{\mathrm{HDA}}=25.8$ mN/m (hexadecylamine), $m_{h0}=1.58$ mg, $m_{\mathrm{HDA}}=1.35\times10^{-2}$ mg, and $\beta=1$. The curve γ_1 describes the evaporation of the NC solution layer with $\gamma_a=24.6$ mN/m (amyl acetate), $\gamma_{\mathrm{NC}}=28.6$ mN/m (cellulose), $m_{a0}=2.15$ mg, $m_{\mathrm{NC}}=2.48\times10^{-2}$ mg, and $\beta=1$. Values of the surface tension γ_{NC}, γ_{HDA}, γ_a, and γ_h are indicated additionally on the right-hand side, respectively. (b) Calculated spreading coefficient S_{21} and interfacial tension between two phases, γ_{21}, as a function of evaporation time, respectively.

acetate. This observation allows us to assume that the evaporation rates of hexane and amyl acetate in our bilayer experiment are almost identical to the rates observed for pure solvents, despite the fact that in the bilayer experiment the top HDA solution layer acts as a diffusion barrier for evaporation of amyl acetate from the bottom layer. From the data of the evaporation rate in the two-phase solvent, we have determined the time dependence of both the thickness d_2 of the HDA solution layer and the thickness d_1 of the NC solution layer in our experiment for each sample investigated. Figure 7(b) shows these dependences for a sample with $h_f=2.7$ nm, where t_2 and t_1 are the time spans necessary to completely evaporate hexane and amyl acetate from the sample, respectively [18]. For each solvent, the mass m_s evaporated with time t, for $0<t<t_0$, can be described as $m_s=m_{s0}(1-t/t_0)$, where m_{s0} denotes the mass of hexane or amyl acetate at $t=0$, respectively. At the starting point of the evaporation process, for hexane, we have $m_{s0}=m_{h0}$ and $t_0=t_2$ and, for amyl acetate, we have $m_{s0}=m_{a0}$ and $t_0=t_1$. The time dependence of the surface tension γ_2 of the binary HDA solution that contains hexane (γ_h) and hexadecylamine (γ_{HDA}) can be calculated as [11]

$$\gamma_2=\gamma_h N_h+\gamma_{\mathrm{HDA}}N_{\mathrm{HDA}}-\beta N_h N_{\mathrm{HDA}}, \tag{1}$$

where β is a semiempirical constant. Here, $N_h=(1-t/t_2)/(1-t/t_2+\alpha)$ and $N_{\mathrm{HDA}}=\alpha/(1-t/t_2+\alpha)$ are fractions of the corresponding component in the binary solution, where $\alpha=m_{\mathrm{HDA}}/m_{h0}$ and m_{HDA} denotes the mass of hexadecylamine in the top layer. Accordingly, Eq. (1) can be used for the NC solution layer that contains amyl acetate and cellulose. Figure 8(a) displays the results calculated for both surface tensions γ_2 and γ_1 versus evaporation time. The corresponding spreading coefficient S_{21} and surface tension γ_{21} versus evaporation time are demonstrated in Fig. 8(b). Obviously, S_{21} is positive until $\gamma_2=\gamma_1$. Only for negative values of S_{21} will the HDA solution dewet the underlying NC solution layer. The line γ_{21} indicates the tension at the interface between the two layers which was calculated via $\gamma_{21}=\gamma_2+\gamma_1-2(\gamma_2\gamma_1)^{0.5}$ [19].

For the following discussion, it is necessary to know how the viscosity of both layers, η_2 and η_1, changes during evaporation. The qualitative behavior of these changes in both binary solution layers can be determined via the Einstein limiting law [11] $\eta=\eta_0(1+2.5\varphi)$. Here, φ is the ratio of the volume of HDA to that of hexane in the top layer, and the ratio of the volume of NC to that of amyl acetate in the lower layer, i.e., $\varphi_2=V_{\mathrm{HDA}}/V_h$ for the HDA solution layer and $\varphi_1=V_{\mathrm{NC}}/V_a$ for the NC solution layer. The change of the solvent volume during evaporation can be evaluated as V_s

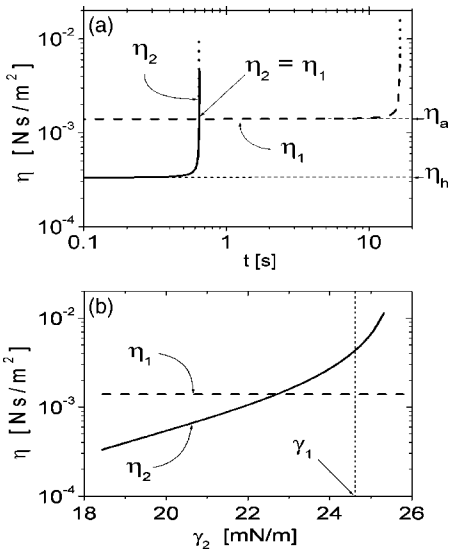

FIG. 9. (a), (b) Calculated viscosities of both layers as a function of evaporation time and as a function of the surface tension of the HDA solution layer, respectively. The line η_2 characterizes the evaporation process of the HDA solution with $\eta_h = 3.26 \times 10^{-4}$ N s/m^2 (hexane), $V_{h0} = 2.4 \times 10^{-3}$ cm^3, and $V_{\mathrm{HDA}} = 1.7 \times 10^{-5}$ cm^3. The line η_1 describes the evaporation of the NC solution with $\eta_a = 1.37 \times 10^{-3}$ N s/m^2 (amyl acetate), $V_{a0} = 2.5 \times 10^{-3}$ cm^3, and $V_{\mathrm{NC}} = 1.9 \times 10^{-5}$ cm^3. Values of η_a and η_h are indicated additionally on the right-hand side, respectively. The vertically dotted line in (b) characterizes the evaporation time at which the values of the surface tension of both HDA solution and NC solution layers are equal, i.e., $\gamma_2 = \gamma_1$.

$= V_{s0}(1 - t/t_0)$, where the values of time t_0 of both layers are the same as in Eq. (1). Figure 9(a) displays the results calculated for the viscosity of both layers, η_2 and η_1, versus evaporation time for the sample with $h_f = 2.7$ nm. The corresponding dependences of both viscosities versus the surface tension of the HDA solution depicted in Fig. 9(b) illustrate that the viscosity of the NC solution was smaller (about a factor 3) than that of the HDA solution at the point where dewetting of the HDA solution layer starts (value $\gamma_2 = \gamma_1 = 24.6$ mN/m indicated by a dotted line).

For the thin HDA solution top layer in a multilayer structure shown in Fig. 6(a), all interactions between the surrounding materials across the HDA solution layer (NC solution layer, air, and water) will contribute to the total excess free energy ΔG_2 of the HDA solution layer [20,21]. If the interactions between the different thin layers in Fig. 6(a) are determined by Lifshitz–van der Waals forces only, the excess free energy ΔG_2 can be evaluated as a sum of two terms which describe the nonretarded interaction between the HDA solution layer and the surrounding media [21],

$$\Delta G_2 = \frac{-1}{12\pi}\left(\frac{A_{124}}{d_2^2} + \frac{A_{0124}}{(d_1 + d_2)^2}\right). \tag{2}$$

The first term describes the interaction between the NC solution layer 1 and air 4 across the HDA solution layer 2, the second term the interaction between the water substrate 0 and air 4 across the layers 1 and 2. The effective Hamaker constants A_{124} and A_{0124} can be composed by the respective Hamaker constants of each medium [20,22],

$$A_{124} = (\sqrt{A_{11}} - \sqrt{A_{22}})(\sqrt{A_{44}} - \sqrt{A_{22}}), \tag{3}$$

$$A_{0124} = (\sqrt{A_{44}} - \sqrt{A_{22}})(\sqrt{A_{00}} - \sqrt{A_{11}}). \tag{4}$$

The thermodynamic stability of the HDA solution layer depends on the sign of the second derivative of ΔG_2 with respect to its thickness d_2 [23–25]. If $\Delta G_2'' = \partial^2 \Delta G_2 / \partial d_2^2$ is negative, the HDA solution layer will be unstable, and spinodal decomposition of this layer occurs. From Eq. (2), it follows that

$$\Delta G_2'' = -\frac{A_{124}}{2\pi d_2^4} - \frac{A_{0124}}{2\pi (d_1 + d_2)^4}. \tag{5}$$

Equation (5) predicts that the behavior of the HDA solution layer depends on the sign of the effective Hamaker constants A_{124} and A_{0124}. Positive Hamaker constants lead to a destabilization of the HDA solution layer, independent of the thickness values d_2 and d_1. Negative values give rise to a stable HDA solution layer, independent of the thickness values d_2 and d_1. If the constants A_{124} and A_{0124} have different signs, the sign of $\Delta G_2''$ can vary with d_2 and d_1.

For the study of the change of the sign of $\Delta G_2''$ during the evaporation, we start by analyzing the behavior of the sign of the constants A_{124} and A_{0124}. The individual Hamaker constants A_{ii} in Eqs. (3) and (4) can be extracted from experimentally determined data of the surface tension γ_{ii} as $A_{ii} = 24\pi\gamma_{ii}(D_o)^2$, with a cutoff intermolecular separation $D_o = 0.165$ nm [19]. At the beginning of evaporation ($t = 0$), the excess free-energy derivative $\Delta G_2'' = 5.8 \times 10^4$ J/m^4 with $d_2 = 381$ nm and $d_1 = 390$ nm [26]. That means the top HDA solution layer is stable at $t = 0$. With the time dependences of the surface tension of both layers $\gamma_2(t)$ and $\gamma_1(t)$ shown in Fig. 8(a) and of their thicknesses $d_2(t)$ and $d_1(t)$ shown in Fig. 7(b), we have determined $\Delta G_2''(t)$ during the evaporation. Figure 10(a) shows that $\Delta G_2''(t)$ becomes negative for $t \geqslant t_{2c} = 0.646$ s, which is 1 ms smaller than time t_2. $\Delta G_2''(t)$ stays negative in the range $0.646\ \mathrm{s} \leqslant t \leqslant 16$ s via the simultaneous change of the parameters $A_{124}(t)$, $A_{0124}(t)$, $d_2(t)$, and $d_1(t)$. Equation (3) shows that a change of the sign from negative to positive values for the constant A_{124} occurs when $A_{22} = A_{11}$ becomes valid, which happens when the surface tension values of both HDA and NC solution layers are equal and dewetting of the top HDA solution layer starts. The effective Hamaker constant A_{0124} is always negative, because the relation $A_{00} > A_{11}$ in Eq. (4) holds during the whole evaporation process. Figure 10(b) demonstrates the change of the constants A_{124} and A_{0124} as a function of evaporation time. In the range where $A_{124} > 0$ and $A_{0124} < 0$, Eq. (5) demonstrates that the stability of the top HDA solution layer depends only on the ratio $|A_{0124}|/A_{124}$. Comparison of the values of $|A_{0124}|$ with that of A_{124} indicates that the ratio $|A_{0124}|/A_{124} > 1$ is valid during the evaporation [see Fig. 10(b)]. Accordingly, the HDA solution layer can be stable or unstable depending only on the thickness values d_2 and d_1.

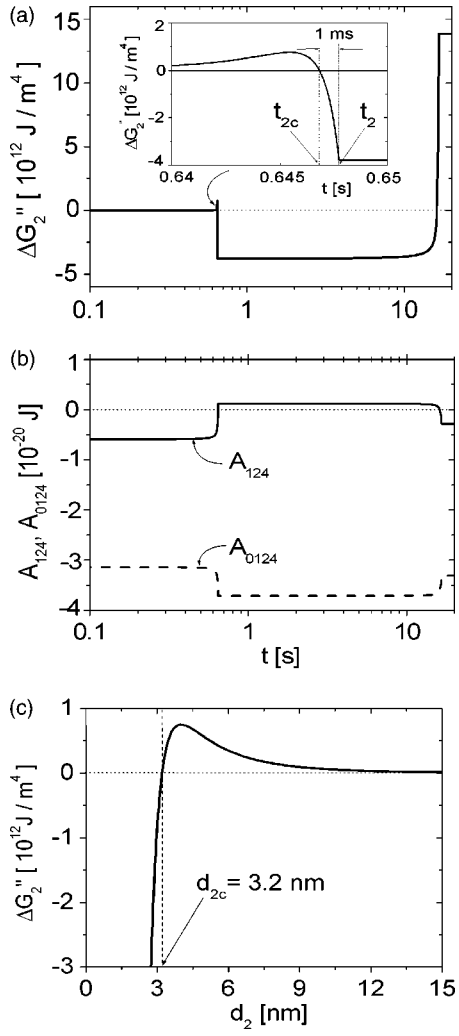

FIG. 10. (a) Calculated second derivative of excess free energy ($\Delta G_2''$) versus evaporation time for the HDA solution layer (for the sample with h_f=2.7 nm). The detailed analysis near the time $t=t_2$ is magnified in the inset. (b) Calculated Hamaker constants A_{124} and A_{0124} versus evaporation time. (c) Calculated $\Delta G_2''$ as a function of thickness d_2 of the HDA solution layer in the range where the rupture of this layer occurs. The characteristic thickness $d_2=d_{2c}$ is the thickness at which the relation $\Delta G_2''=0$ is valid.

The thickness $d_2=d_{2c}$ at which Eq. (5) becomes zero and, correspondingly, the relation $\Delta G_2''$ becomes negative can be calculated from Eq. (5) as

$$d_{2c} = \frac{d_1}{\left(\frac{|A_{0124}|}{A_{124}}\right)^{1/4} - 1}. \tag{6}$$

With $\Delta G_2''(t)$ shown in Fig. 10(a) and $d_2(t)$ shown in Fig. 7(b), we determined the dependence of $\Delta G_2''$ as a function of d_2. Figure 10(c) shows that the thickness $d_2=d_{2c}$, where $\Delta G_2''$ becomes negative, amounts to 3.2 nm for the sample with h_f=2.7 nm. That means the thickness $d_2=d_{2m}$ at which the decomposition of the HDA solution layer takes place is located in the range from 2.7 nm to 3.2 nm.

The stability of thin films of nonvolatile liquids was theoretically considered, in general, by Vrij and Overbeek [24,25], and later by Brochard-Wyart *et al.* [27] also for the case of liquid substrates. The latter model predicts the development of a peristaltic mode of a liquid film deposited on the other thin liquid if the thickness of both layers is small compared to the wavelength of their modulations. The modulations of both interfaces of the top liquid film develop in antiphase. In a recent theoretical work [28], the stability of two superposed ultrathin layers of different liquids on a solid substrate depending on the ratio of the layer thicknesses was looked at. It was shown that if the top layer is thinner than the lower one, two interfaces start to evolve modulations that are in antiphase. On the contrary, if the top layer is thicker than the lower one, the modulations of the two interfaces are in phase. Taking advantage of these results [27,28], in order to describe the thickness modulations of the HDA solution layer in our bilayer structure where the thickness d_2 is essentially smaller than d_1, the corresponding modulations of the thickness d_2 can be illustrated as shown in Fig. 6(b). The modulations of both interfaces induce a Laplace and a disjoining pressure gradient in the HDA solution layer, leading to some flow of both liquids J_2 and J_1, as shown in Fig. 6(b).

In the instability model [24,25,27], the thermally induced thickness modulations grow exponentially in amplitude if their wave vector q is less than the critical vector q_c, while the amplitude of the modulations with $q>q_c$ decreases with time. The corresponding critical wavelength of the in-plane surface modulations is determined as $\lambda_c=2\pi/q_c$ [see Fig. 6(b)]. The fastest growing modulation, which will lead to rupture of the HDA solution layer, occurs if the wavelength λ reaches the characteristic value $\lambda_m=\lambda_c\sqrt{2}$ [24,25]. The corresponding characteristic time τ_m necessary to rupture the HDA solution layer can be calculated as [24,28] $\tau_m=48\pi^2\eta_2\gamma_2 d_{2m}^5/A_{124}^2=0.1$ s with $d_{2m}=3$ nm, $\gamma_2=25.06$ mN/m, $\eta_2=7.2\times10^{-3}$ N s/m^2, and $A_{124}=4.39\times10^{-22}$ J. That means the time $\tau_m=0.1$ s is significantly smaller than the total time span (15.35 s) during which the HDA solution layer is in the unstable regime, i.e., the relation $\Delta G_2''<0$ holds [Fig. 10(a)].

For $\Delta G_2''<0$, the characteristic wavelength λ_m and $\Delta G_2''$ are connected via the equation [24,25]

$$\lambda_m(d_{2m}) = [-8\pi^2\gamma_2(d_{2m})/\Delta G_2''(d_{2m})]^{1/2}. \tag{7}$$

With $\Delta G_2''=-3.78\times10^{12}$ J/m^4, which is valid during the evaporation time from 0.646 s to 16 s [see Fig. 10(a)], and with $\gamma_2=25.06$ mN/m ($d_{2m}=3$ nm), we obtain the characteristic wavelength $\lambda_m=720$ nm. The experimentally observed value of the interdroplet distance $\lambda_{md}=1380$ nm turns out to be about a factor of 2 larger than λ_m for the sample with the droplet diameter $D_d=950$ nm ($h_f=2.7$ nm). One would expect [see Fig. 6(b)] that the wavelength λ_m must be equal to the measured interdroplet distance λ_{md} shown in Fig. 2(b), if the dynamical effects during decomposition are negligible. The diameter of the fluid droplets formed directly after decomposition of the HDA solution layer will be about the size of the wavelength λ_m, but subsequent evaporation of the solvent from the droplets leads to a shrinking of their diameter, i.e., the measured droplet diameter D_d must always be

smaller than λ_m. Comparing the calculated and experimental values, we assume that the difference between λ_m, λ_{md}, and D_d can be explained with a possible coalescence of HDA droplets formed directly after rupture of the HDA solution layer into larger droplets, which are the only ones we have observed at the end of the evaporation process [Fig. 2(a)].

In accordance with Eqs. (5) and (7), the characteristic wavelength λ_m of the critical modulations at the moment the HDA solution layer decomposes into droplets is proportional to d_{2m}^2, which is in good agreement with the experimental dependence $\lambda_{md} \propto h_f^{2.03}$ illustrated in Fig. 5(a). The experimentally determined dependence $\lambda_{md} \propto D_d^{1.21}$ indicates an approximately linear change of λ_{md} with the droplet diameter D_d [Fig. 4(a)] and supports our proposed mechanism of droplet pattern formation shown in Fig. 6(b). The latter explains the almost linear dependence $h_d \propto h_f^{1.19}$ [Fig. 5(b)]. Taking further advantage of the dependences $\lambda_{md} \propto h_f^{2.03}$ and $\lambda_{md} \propto D_d^{1.21}$, we calculated the dependence $h_d \propto D_d^{0.71}$, which is in good agreement with the measured value $h_d \propto D_d^{0.86}$ [Fig. 4(b)]. That means that the power-law fit used in Fig. 4(b) to describe the stepwise dependence $h_d(D_d)$ is more or less correct. The stepwise character of the change of h_d with the droplet diameter derives from the fact that the HDA molecules form micelles. According to Eqs. (5) and (7), $\lambda_m \propto d_{2m}^2$ and, therefore, the area per liquid droplet is proportional to d_{2m}^4. Correspondingly, the droplet number N_d per sample area (in our case, 100 μm^2) must be proportional to d_{2m}^{-4}. Comparing this prediction with the experimentally determined dependence $N_d \propto h_f^{-3.46}$ [Fig. 5(d)], the agreement appears reasonable. Conservation of the HDA mass, assuming that a layer with thickness h_f and area λ_{md}^2 is transformed into a droplet with thickness h_d and diameter D_d, is described via $\lambda_{md}^2 h_f \propto D_d^2 h_d$. With $\lambda_{md} \propto h_f^{2.03}$ and $h_d \propto D_d^{0.86}$, it follows that $D_d \propto h_f^{1.75}$. The measured dependence $D_d \propto h_f^{1.59}$ [Fig. 5(c)] is in good agreement with the expected one.

Our model for rupturing the HDA solution layer, as sketched in Fig. 6, was further supported via a complementary experiment which must demonstrate an experimental confirmation of the bilayer formation in a thin film of the binary solution onto the water substrate. In other words, with this experiment we want to register the formation of a bilayer structure onto the water surface as a sequence of separate layer formation. For that purpose, we used spin coating of two- and one-phase solutions on the Si substrate, because the separate HDA layer cannot be produced via the spreading of the solution onto the water substrate, initially covered with the NC film. First, we have spin-coated a mixed solution containing 50% of a 0.1% NC solution in amyl acetate and 50% of a 0.1% HDA solution in hexane onto a Si substrate. The AFM image in Fig. 11(a) shows that a phase-separated structure of HDA clusters has been developed on the cellulose layer. The thickness of the clusters amounts to about 3 nm [Fig. 11(b)]. Due to the removal of the HDA clusters from the sample (by immersing the sample in hexane), we have found that the HDA clusters were located on the surface of the cellulose layer and they have no contact with the Si substrate. Second, we have spin-coated a 0.05% HDA solution in hexane onto a Si substrate covered first with a nitrocellulose film. The resulting AFM image illustrated in Fig. 11(c) discloses a similar [compared to that of Fig. 11(a)] structure of HDA clusters on the cellulose layer. The thickness of the clusters amounts to about 3 nm [Fig. 11(d)]. The obvious similarity between both structures in Figs. 11(a) and 11(c) can be explained only with the following effect. In the first case, the initial thin layer of mixed solutions on the Si substrate by spin coating transforms into a bilayer structure which consists of a hexane/hexadecylamine solution layer at the solution-air interface and an amyl acetate/cellulose solution layer at the solution-substrate interface. The total thickness of the fluid film prepared by spin coating amounts to about 1 μm. That means, in the first case, that spin coating of the mixed solution provides a thickness of the top HDA solution layer of about 0.5 μm and a thickness of the lower NC solution layer of about 0.5 μm. As a result, the mass of HDA in the top layer of the first case (0.1% HDA solution) turns out to be about equal to the mass of HDA in the layer of the second case (0.05% HDA solution), eventually producing similar structures of the HDA clusters in both cases. The latter finding agrees with those described above for droplet formation (see Fig. 6).

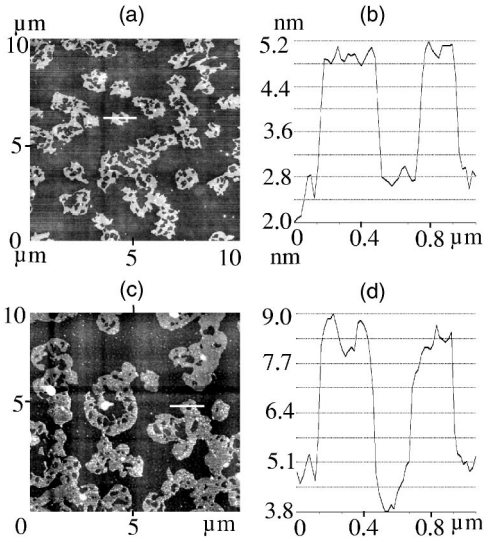

FIG. 11. (a) AFM image of HDA clusters formed by spin coating of a blend that contains 50% of a 0.1% nitrocellulose solution in amyl acetate and 50% of a 0.1% hexadecylamine solution in hexane onto a Si substrate. (b) AFM profile of the scan line indicated in (a). (c) AFM image of HDA clusters formed by spin coating of a 0.05% hexadecylamine solution in hexane onto a Si substrate covered first with a cellulose film. (d) AFM profile of the scan line indicated in (c).

V. CONCLUSION

Phase separation of a binary solution on a water surface leads to the formation of a bilayer structure which consists of an HDA solution layer at the solution-air interface and a NC solution layer at the solution-water interface. Evaporation of the solvent from both layers gives rise to a fast thickness decrease of the top HDA solution layer, while the lower NC

solution layer changes much more slowly. The thermodynamic stability of the HDA solution layer depends on the sign of the second derivative of the excess free energy $\Delta G_2''$ with respect to its thickness. For $\Delta G_2'' < 0$, the HDA solution layer will be unstable such that it decomposes into droplets. We found that the calculated wavelength of the thickness modulations of the HDA solution layer is in good agreement with experimentally determined geometrical parameters of the resulting pattern such as droplet height, droplet diameter, interdroplet distance, and number of droplets per unit sample area.

ACKNOWLEDGMENTS

This work was financially supported by the Energieversorgung Weser-Ems Foundation (Project 04.041) and by the European Science Foundation (COST P12).

[1] Y. Cui, Q. Wei, H. Park, and C. M. Lieber, Science **293**, 1289 (2001).
[2] P. C. Ohara and W. M. Gelbart, Langmuir **14**, 3418 (1998).
[3] V. Kurikka, P. M. Shafi, I. Felner, Y. Mastai, and A. Gedanken, J. Phys. Chem. **103**, 3358 (1999).
[4] M. Maillard, L. Motte, and M. P. Pileni, Adv. Mater. (Weinheim, Ger.) **13**, 200 (2001).
[5] S. L. Tripp, S. V. Pusztay, A. E. Ribbe, and A. Wei, J. Am. Chem. Soc. **124**, 7914 (2002).
[6] D. Wyrwa, N. Beyer, and G. Schmid, Nano Lett. **2**, 419 (2002).
[7] L. V. Govor, G. Reiter, G. H. Bauer, and J. Parisi, Appl. Phys. Lett. **84**, 4774 (2004).
[8] L. V. Govor, G. Reiter, J. Parisi, and G. H. Bauer, Phys. Rev. E **69**, 061609 (2004).
[9] E. Shevchenko, D. Talapin, A. Kornowski, A. Rogach, and H. Weller, J. Am. Chem. Soc. **124**, 11480 (2002).
[10] L. V. Govor, I. A. Bashmakov, R. Kiebooms, V. Dyakonov, and J. Parisi, Adv. Mater. (Weinheim, Ger.) **13**, 588 (2001).
[11] A. W. Adamson, *Physical Chemistry of Surfaces* (Wiley, New York, 1982).
[12] L. V. Govor, G. H. Bauer, G. Reiter, E. Shevchenko, H. Weller, and J. Parisi, Langmuir **19**, 9573 (2003).
[13] F. Bruder and R. Brenn, Phys. Rev. Lett. **69**, 624 (1992).
[14] U. Steiner, J. Klein, and L. J. Fetters, Phys. Rev. Lett. **72**, 1498 (1994).
[15] W. Straub, F. Bruder, R. Brenn, G. Krausch, H. Bielefeldt, A. Kirsch, O. Marti, J. Mlynek, and J. F. Marko, Europhys. Lett. **29**, 353 (1995).
[16] K. Tanaka, A. Takahara, and T. Kajiyama, Macromolecules **29**, 3232 (1996).
[17] W. A. Zisman, *Contact Angles, Wettability, and Adhesion*, Advanced Chemistry Series Vol. 43 (ACS, Washington, DC, 1991).
[18] For example, for the evaporation of hexane out of the sample with $d_2 = 381$ nm ($h_f = 2.7$ nm), we obtained a time span $t_2 = 0.647$ s; for the evaporation of amyl acetate out of this sample with $d_1 = 390$ nm, we obtained a time span $t_1 = 16.58$ s.
[19] J. N. Israelachvili, *Intermolecular and Surface Forces* (Academic Press, London, 1991).
[20] J. Visser, Adv. Colloid Interface Sci. **3**, 331 (1972).
[21] I. B. Ivanov, *Thin Liquid Films: Fundamentals and Applications* (Marcel Dekker, New York, 1988).
[22] D. Bargeman and F. van Voorst Vader, J. Electroanal. Chem. Interfacial Electrochem. **37**, 45 (1972).
[23] A. Scheludko, Adv. Colloid Interface Sci. **1**, 391 (1967).
[24] A. Vrij, Discuss. Faraday Soc. **429**, 23 (1966).
[25] A. Vrij and J. Th. G. Overbeek, J. Am. Chem. Soc. **90**, 3074 (1968).
[26] At the evaporation time $t = 0$, we obtain the constants $A_{22} = 3.8 \times 10^{-20}$ J, $A_{11} = 5.0 \times 10^{-20}$ J, and $A_{00} = 1.5 \times 10^{-19}$ J for experimentally obtained values of $\gamma_2 = 18.4$ mN/m, $\gamma_1 = 24.6$ mN/m, and $\gamma_0 = 72.5$ mN/m, respectively. The Hamaker constant of air is $A_{44} = 0$. For the above values attributed to the parameters in Eqs. (3)–(5), the effective Hamaker constants are $A_{124} = -0.6 \times 10^{-20}$ J and $A_{0124} = -3.1 \times 10^{-20}$ J.
[27] F. Brochard-Wyart, P. Martin, and C. Redon, Langmuir **9**, 3682 (1993).
[28] A. Pototsky, M. Bestehorn, D. Merkt, and U. Thiele, Phys. Rev. E **70**, 025201(R) (2004).